

NATO Science for Peace and Security Series - B:
Physics and Biophysics

Fundamental and Applied Nano-Electromagnetics II

THz Circuits, Materials, Devices

Edited by
Antonio Maffucci
Sergey A. Maksimenko



Springer



*This publication
is supported by:*

The NATO Science for Peace
and Security Programme

Proceedings of the NATO Advanced Research Workshop on Fundamental
and Applied NanoElectroMagnetics II: THz Circuits, Materials,
Devices Minsk, Belarus
5–7 June 2018

ISBN 978-94-024-1689-3 (PB)

ISBN 978-94-024-1689-3 (HB)

ISBN 978-94-024-1687-9 (e-book)

<https://doi.org/10.1007/978-94-024-1687-9>

Published by Springer,
P.O. Box 17, 3300 AA Dordrecht, The Netherlands.

www.springer.com

Printed on acid-free paper

All Rights Reserved

© Springer Nature B.V. 2019

This work is subject to copyright. All rights are reserved by the Publisher, whether the whole or part of the material is concerned, specifically the rights of translation, reprinting, reuse of illustrations, recitation, broadcasting, reproduction on microfilms or in any other physical way, and transmission or information storage and retrieval, electronic adaptation, computer software, or by similar or dissimilar methodology now known or hereafter developed.

The use of general descriptive names, registered names, trademarks, service marks, etc. in this publication does not imply, even in the absence of a specific statement, that such names are exempt from the relevant protective laws and regulations and therefore free for general use.

The publisher, the authors, and the editors are safe to assume that the advice and information in this book are believed to be true and accurate at the date of publication. Neither the publisher nor the authors or the editors give a warranty, express or implied, with respect to the material contained herein or for any errors or omissions that may have been made. The publisher remains neutral with regard to jurisdictional claims in published maps and institutional affiliations.

Chapter 8

First- and Second Order Light Scattering Processes in Biological Photonic Nanostructures



Géza I. Márk, Krisztián Kertész, Gábor Piszter, Zsolt Bálint,
and László P. Biró

Abstract The colors of various butterflies often originate from photonic nanostructures, found in the scales covering their wings. Such colors are called structural colors. The color generating scales are composed of a nanostructured chitinous material containing air voids, which causes the structural colors through light interference. We performed optical spectrum simulations utilizing full 3D Maxwell equation calculations on model structures to reveal the connection between the 3D structure and the optical spectrum. Our simulations showed that different scattering processes determine the spectrum in different wavelength ranges. For large wavelengths (>350 nm) the optical reflection can be well described by a corresponding effective multilayer model and the peak positions are well represented by a simple first Born approximation. One has to include second order scattering processes inside the layers, however, in order to correctly reproduce the small wavelength side of the spectrum (<350 nm). This means that such details of structure, as the shape of the air voids determine the small wavelength spectrum.

Keywords Photonic crystals · Bioinspiration · First born approximation · Ewald sphere

G. I. Márk (✉) · K. Kertész · G. Piszter · L. P. Biró
Institute of Technical Physics and Materials Science, Centre for Energy Research,
Budapest, Hungary
e-mail: mark@mfa.kfki.hu

Z. Bálint
Hungarian Natural History Museum, Budapest, Hungary

© Springer Nature B.V. 2019
A. Maffucci, S. A. Maksimenko (eds.), *Fundamental and Applied Nano-Electromagnetics II*, NATO Science for Peace and Security Series B: Physics and Biophysics, https://doi.org/10.1007/978-94-024-1687-9_8

8.1 Introduction

The colors of animals [1] originate from pigments and photonic nanostructures, often from a complex interplay between them. Even when the optical properties of the materials building up photonic nanostructures do not show significant wavelength dependence in bulk form, the reflection function of the nanostructure can still show wavelength dependence. Colors originating from photonic nanostructures are called structural colors, and their most spectacular examples are seen on insects, beetles and butterflies. The most prominent optical phenomenon seen in butterfly wings is the so-called iridescence, [2] when the hue of the butterfly wing changes with the angle of observation and/or illumination. Butterfly wings are covered by scales, which are flat sacs of dried cuticle. The spatial dimension of a wing scale is limited, its thickness is generally only 1–2 μm and its lateral extension is 50–100 μm . While the lower – closer to the wing membrane – side is generally structureless, the upper side may have a complicated structure. The inside of the scale is often filled by nanostructured chitinous material, which causes [3] the structural colors by constructive and destructive interference of the electromagnetic waves scattered on these microstructures or nanoarchitectures. This nanostructured chitinous material is a nanocomposite built of mostly two basic components with different refraction indices [4, 5], air $n_{\text{air}} = 1$ and chitin, $n_{\text{chitin}} = 1.56$. The air is present in the system in the form of air voids with sizes and distances such that the reflection spectrum of the scale has peaks in the visible wavelength range, which is perceived as a structural color [6].

Butterfly scale microstructures can be classified by a number of ways, [vii] a detailed classification from the point of view of biology was given by Ghiradella [7, 8]. One of the simplest classification of the nanoarchitectures found in butterfly scales from a physicist's point of view is whether it has a structure in the length scale of the wavelength of visible light in one, two, or all the three dimensions (1D, 2D, and 3D structures). Optical properties of butterfly wing scales were first modeled by the theoretical concept of photonic crystal, [9] which, in its most general definition is a graded-refraction-index material, where the refractive index is a periodic function of the displacement in one-, two-, or three dimensions, giving rise to a stop band. The stop band, or photonic band gap, an analogue of the forbidden band in solid state physics, is a wavelength range where light can not travel through the crystal, hence it is reflected. Biological materials, however, always have certain kind of disorder and the disorder varies on a large scale among different butterfly species. Crystalline order, however, is not a necessary condition of the existence of photonic band gap, amorphous materials can also have [10] a photonic band gap, if a short-range order is present. Metallic-like reflectance, i.e., emergence angle selection is related to the photon momentum conservation, which follows from total or partial translational invariance in the diffusing surface structure. Hence the metallic-like

reflectance is associated with highly correlated structures [2, 11]. It is remarkable, however, that not only shiny, but also matt appearance can be produced by scale nanostructures [12]. Matt appearance seems to always involve some form of long-range disorder. Both the shiny reflectance and the diffuse reflectance have specific biological function for the individual. Shiny reflectance is used for signaling, which is crucial for sexual communication, therefore the color is under sexual selection. The matt color has a cryptic function serving as a generalized camouflage function, thus affected by natural selection [13].

Most important tools to analyze the nanostructure of butterfly wing scales are scanning electron microscopy (SEM) and transmission electron microscopy (TEM). Top-view SEM images provide information, however, about the topmost layer only and the sample preparation (deposition of sputtered gold) may distort the appearance of the nanostructures on the images. Cross-sectional TEM images do give access to the in-depth structure of the scales, but the precise direction of the cut is generally not known—an uncertainty of $5\text{--}10^\circ$ is common—and the samples are sometimes distorted during the preparation process. Both methods give basically 2D information and it is a non trivial task to determine the real 3D structure of the scale based on SEM and TEM images. A careful correlated examination of the SEM and TEM images [12] has to be carried out in order to obtain the full 3D structure.

Computational electrodynamics [14] can predict the optical properties of a material of known three-dimensional structure with high accuracy, utilizing frequency domain methods, such as the Finite Element Method (FEM), or time domain methods, such as the Finite-Difference Time-Domain Method (FDTD). These computations give exact results for perfectly ordered structures, but do have difficulties in handling randomness, because of the large computational demand. Butterfly wing scales, however, have a small refractive index contrast, small thickness, and low absorption. Hence it is possible to approximate their optical properties by simpler, but more intuitive methods, such as first order scattering methods.

In this Chapter we demonstrate the applicability and limitations of the first order scattering method for approximate calculation of the optical properties of butterfly wing scales. The organization of this Chapter is as follows. In Sect. 8.2 we review the basic formulas of the first order scattering method and demonstrate it on examples utilizing the Ewald sphere construction. In Sect. 8.3 we investigate in detail, how the randomness, which is inherently present in the nanoarchitectures of biological origin, influences the light scattering process. By systematic analysis of different distortions of a perfect lattice we identify the signatures of disorder in the Fourier power spectrum. In Sect. 8.4. we apply these principles to real butterfly photonic nanostructures. Section 8.5 contains a comparison of the reflection spectrum calculated by full 3D electrodynamics with the first order approximation. Here we introduce the concept of second order scattering. Section 8.6 is devoted to the conclusions.

8.2 The First Born Approximation and the Ewald Sphere Method

The first order scattering intensity, according to basic scattering theory, [15] is given by

$$I(\vec{k}; \vec{k}_0) = \int \rho(\vec{r}) \exp\left(i \frac{\vec{q}}{n_{eff}} \cdot \vec{r}\right) d^D \vec{r}, \quad (8.1)$$

where $\rho(\vec{r})$ is the density of the scattering centers, \vec{k}_0 is the wave vector of the incoming light, \vec{k} is the wave vector of the outgoing (transmitted or reflected) light, (the magnitude of the two wave vectors is equal in case of elastic scattering), $\vec{q} = \vec{k} - \vec{k}_0$ is the scattering vector, and n_{eff} is the effective refractive index of the medium. The integral is a D dimensional integral, $D = 3$ in 3D calculations, but it is $D = 2$ in the 2D examples demonstrated in this section. This exponential integral has the same form as a Fourier integral and this is the basis of the so called Ewald construction, demonstrated in Fig. 8.1 which is widely used in the theory of elastic X-ray scattering. Figure 8.1a shows a hypothetic 2D periodic $\rho(x, y)$ distribution of the scattering centres and Fig. 8.1b its Fourier transform $\tilde{\rho}(k_x, k_y)$. The $\rho(x, y)$ is periodic, hence $\tilde{\rho}(k_x, k_y)$ consists of discrete points (Dirac deltas) – which become square pixels in the quantized numerical representation (Discrete Fourier Transform, DFT) of Fig. 8.1b. The $\rho(x, y)$ is, however, not harmonic (not a

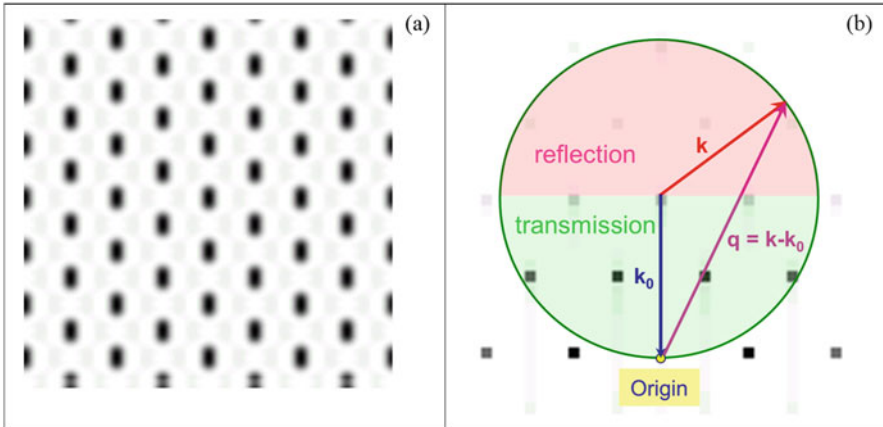


Fig. 8.1 Demonstration of the Ewald construction in two dimensions. (a) A simulated triangular periodic lattice (sum of three anharmonic plane waves in 120^0 directions). (b) Fourier transform of the lattice in (a) and the Ewald construction. \vec{k}_0 is the wave vector of the incoming light, \vec{k} is the wave vector of the outgoing (transmitted or reflected) light, (the magnitude of the two wave vectors is equal in case of elastic scattering), $\vec{q} = \vec{k} - \vec{k}_0$ is the scattering vector

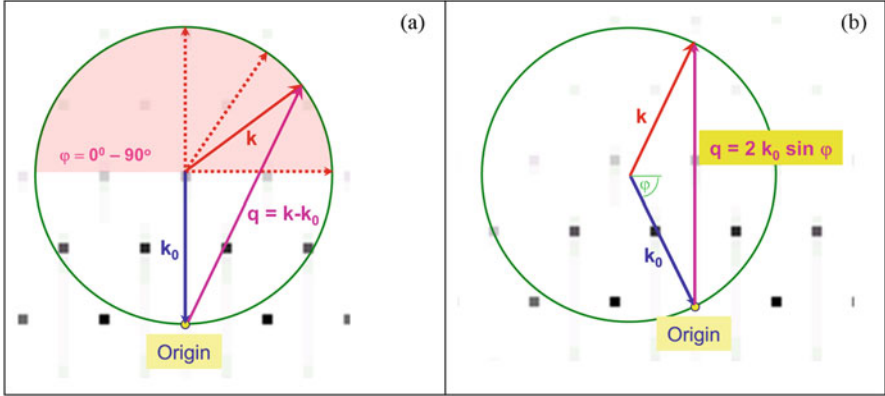


Fig. 8.2 Ewald construction for different cases. (a) When the angle of the outgoing light changes between 0–90° (from perpendicular scattering to normal backscattering), the length of the scattering vector changes from $q_{min} = \sqrt{2}k_0$ to $q_{max} = 2k_0$. (b) Specular (mirror) reflection. The length of the scattering vector depends on the incoming (=outgoing) angle as $q = 2k_0 \sin \varphi$

sinusoidal function), hence several harmonics (“overtones”) are seen in $\tilde{\rho}(k_x, k_y)$. If the sample is illuminated with a monochromatic plane wave with wave vector \vec{k}_0 and we detect the light scattered in different directions, then the tip of the wave vector \vec{k} of the scattered light moves along a sphere (a circle in 2D), because the scattering is elastic, hence $|k| = |k_0| = \frac{2\pi}{\lambda}$. This is called the Ewald sphere (circle). The scattered light intensity $I(\vec{k}; \vec{k}_0)$ in different directions is given by the value of the $\tilde{\rho}(k_x, k_y)$ along the Ewald circle. If the incoming light is white light, then different colors are scattered in different directions, as shown on Fig. 8.2a. Figure 8.2b shows the case of the specular (mirror) reflection.

When $\rho(x, y)$ is periodic, then the scattering occurs only in a few directions. This is demonstrated on two three dimensional (3D) examples of Fig. 8.3. In the first example, Fig. 8.3a the lateral arrangement of the scattering centers is a harmonic triangular function and its Fourier transform, Fig. 8.3b is a hexagon of 6 dirac delta peaks. In Fig. 8.3a an infinite number of such layers is stacked in the vertical direction, and the Fourier transform Fig. 8.3b contains also an infinite number of layers, because of the infinitesimal thickness of the layers in Fig. 8.3a. In the second example, Fig. 8.3c the real space function is harmonic in all directions, hence its Fourier transform, Fig. 8.3d is composed only of a finite number of Dirac delta peaks: two hexagons shifted in the z directions. Figure 8.3e shows again these two hexagons together with the Ewald sphere. If we illuminate this sample with a white light in the perpendicular direction there will be a wavelength and direction selection. If we vary the diameter of the Ewald sphere (different colors) it only touches the upper hexagon only for a specific diameter (color) and the scattering

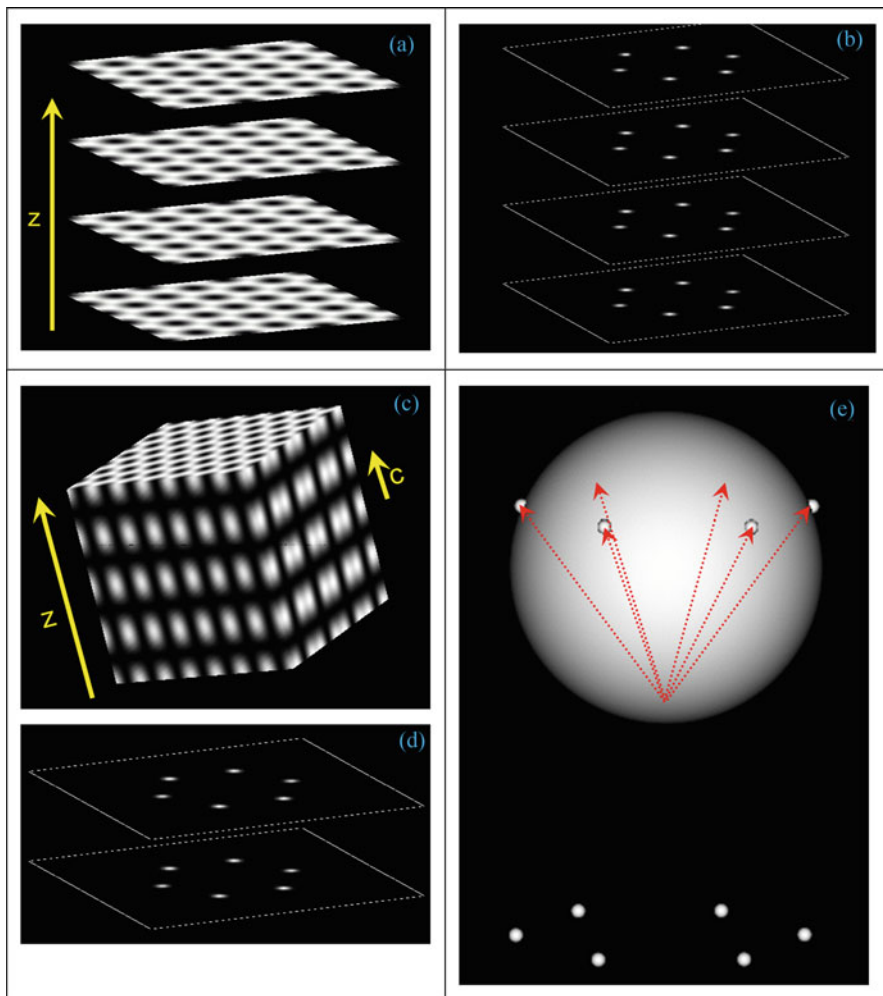


Fig. 8.3 Three dimensional Ewald construction for different cases. **(a)** Layers of harmonic triangular lattices stacked in the vertical (z) direction. The figure shows only 4 layers of the infinite stack. **(b)** Fourier transform of **(a)**. It is composed of infinite number of layers having 6 points in a hexagonal orientation. Only 4 layers are shown. **(c)** A $\rho(x, y, z)$ function harmonic in all three directions. The figure shows only a rectangular volume cut from of the infinite function. **(d)** Fourier transform of **(c)**. It is composed only of two hexagons. **(e)** 3D Ewald construction. Backscattering occurs only for one color and six angles determined by the periodicities of $\rho(x, y, z)$

directions of this color are determined by the touching points (denoted by the six red vectors in Fig. 8.3e). It is interesting that there is no forward scattering (transmittance) in this system because the Ewald sphere does not cross the lower hexagon whatever the diameter is.

8.3 Order-Disorder Effects in the First Order Scattering

The model geometries analyzed in Sect. 8.2. were perfect infinite crystal structures, possessing a perfect translational symmetry. If a structure has a perfect long range order, its Fourier transform is composed of distinct peaks. This situation, is seen in X-ray scattering images in solid state physics, because atomic or molecular crystals can have very regular structures. Photonic nanostructures found in biological systems differ from this ideal situation in two aspects:

1. The structure has a finite size, especially its thickness (z direction) is limited, only several microns. Cutting an infinite structure to a finite size corresponds to a convolution of the Fourier transform of the infinite structure with the Fourier transform of the window function (e.g. $\sin x/x$ for the case of a rectangular window).
2. Biological systems always contain disorder. If the real space structure is not as regular as crystals in solid state physics, the Fourier transform is not any more composed of Dirac delta like peaks, but it has a complicated, continuous distribution in reciprocal space.

First we analyze the effect of the finite size. Figure 8.4 shows the effect of the spatial confinement of the system, it is composed only of four layers, but the layers are assumed to be infinite in the x direction. As seen on Fig. 8.4b and d, the Fourier peaks are broadened in the y direction and satellite peaks appear between the original peaks. For the case of n layers there are $n-1$ zero nodes and $n-2$ satellite peaks. Figure 8.4c is a function constructed as a sum of four Gaussians placed on an equidistant grid and Fig. 8.4d shows its Fourier power spectrum, which is a convolution of a Gaussian with a $\sin x/x$ function. We can see three zero nodes and two maxima. This process is analyzed in detail in [16].

Next we turn to the investigation of the randomness. The upper left subimage of Fig. 8.5 shows a rectangular section of a perfectly regular and infinite 2D square lattice and its Fourier power spectrum. The Fourier image is a square lattice of distinct peaks. The intensity of the peaks is decreasing with the distance from the origin, this decrease is faster if the objects placed on the lattice points of the real space lattice are larger. As we now from the theory of X-ray scattering, if N objects are placed in the points of a direct space lattice, the total scattering of the system is given as the product of the lattice factor (Fourier transform of the lattice) and the so called atomic form factor (Fourier transform of the repeated pattern). The Fourier image is composed of distinct peaks in the horizontal (vertical) direction if the lattice has a long range periodicity in the x (y) direction.

We introduce two different randomness into this “perfect” picture:

- We preserve the perfect periodicity inside the layers, but the lattice layers are randomly displaced horizontally. This is shown in the upper row of Fig. 8.5, for increasing displacements. We can see that the Fourier images are composed of *vertical* lines. This is because the random displacement of the layers destroys the

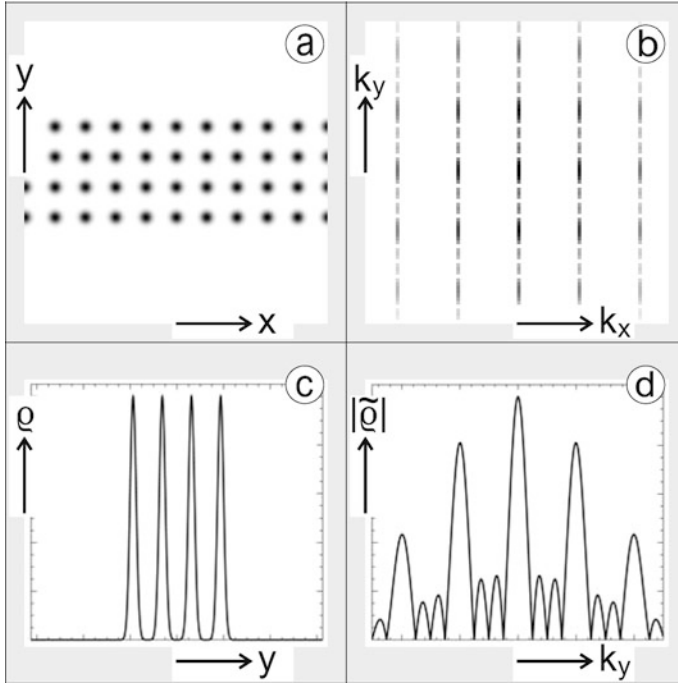


Fig. 8.4 Effect of the finite number of layers on the Fourier power spectrum. (left) Real space images. (right) Reciprocal space images. (a) and (b) Four layers of a perfect rectangular lattice. The structure is infinite in the x direction, only a finite section is shown. (c) Vertical density distribution $\rho(x=0, y)$ in the central column of (a). (d) Vertical Fourier power density distribution $\tilde{\rho}(k_x=0, k_y)$ in the central column of (b). Dimensionless units are used in all subimages. See the text for details

perfect translational symmetry in y . The image is still composed of discrete lines, because the layers still have a perfect translational order in the x direction.

- The leftmost column of Fig. 8.5 shows the effect of the disorder present in the layers themselves. This time a random horizontal displacement with a Gaussian distribution was applied to the points of one layer and this layer was repeated infinitely in the y direction. All of the layers have the same structure this time. The Fourier image shows distinct *horizontal* lines. Indeed, each reciprocal lattice point is broadened in the x direction because of the random x displacement of the points, but the translational order is present in the y direction because the layers have an identical structure.
- The inner subimages of Fig. 8.5 display the effect of applying the two kind of randomizations together. We have here both vertical and horizontal broadening of the Fourier peaks at hand.

Another important kind of random structure is the polycrystalline arrangement, this is shown on Fig. 8.6. First we created a perfect harmonic triangular lattice

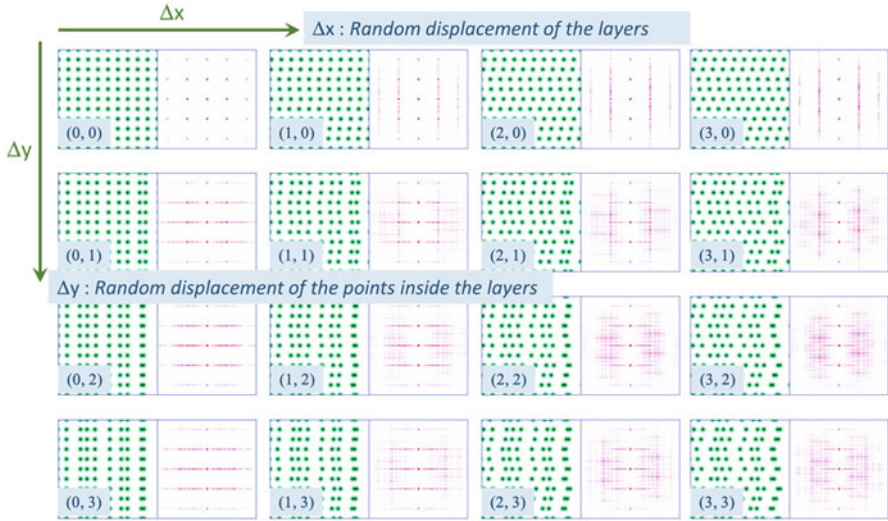


Fig. 8.5 Effect of the randomness on the Fourier power spectrum. The left panes of each subimages show a real space lattice and the right panes show its Fourier power spectrum. The real space lattices are infinite in the calculations, but only a finite window is shown. The subimages are arranged in a matrix, where the columns and the rows corresponds to two different randomization parameters. The upper left subimage is a perfect square lattice. The upper row shows the effect of the random displacement of the layers with increasing displacement from left to right. The leftmost column shows the effect of the random displacement of the points inside the layers with displacement increasing from up to bottom. The inside images are for the combination of both kind of randomization – the reciprocal lattice peaks are broadened in both the vertical and horizontal direction

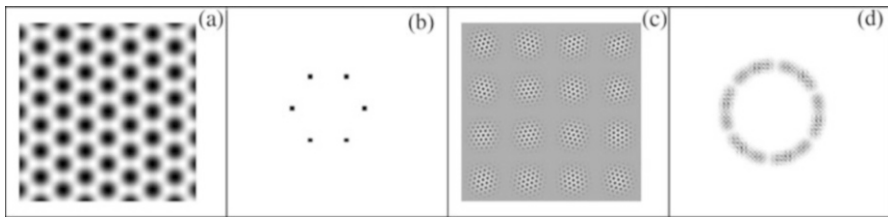


Fig. 8.6 Fourier transform of a polycrystalline lattice. (a) A harmonic triangular lattice. (b) Fourier transform of (a) – six points at the vertices of a hexagon. (c) Polycrystalline lattice. (d) Fourier transform of the polycrystalline lattice

(Fig. 8.6a), its Fourier transform (Fig 8.6b) contains only six points at the vertices of a hexagon. Next we cut (by a 2D Gaussian window function) a finite part of the crystal lattice and placed it to the points of a rectangular superlattice. Then we applied random rotations to each of these “crystallites”. The resulting real space polycrystalline lattice if shown on Fig. 8.6c and its Fourier transform on Fig. 8.6d. The points building up this Fourier image are arranged along a circle. This is because of the rotation invariance and additivity of the Fourier transform: if we rotate the real

space image, then the Fourier image is also rotated with the same angle. Hence the Fourier image of each “crystallites” is a hexagon with a random rotation. The sum of the rotated hexagons gives the circle. The radial broadening of the circle is because of the finite size of the crystallites.

8.4 First Born Optical Spectrum Calculations for Butterfly Scales

The results obtained in Sect. 8.3 makes us able to perform optical spectrum calculations for real butterfly scales and understand the results. Calculations in this Section are based on the method of [17]. They first calculate the two-dimensional Fourier power spectrum (2D FFT) of the binarized TEM image then they estimate the reflectance spectrum by angular averaging of the power spectrum for the whole $[0, 2\pi)$ range or for $\pi/6$ wide sections. We analyze two examples in this section: (i) *Albulina metallica* butterfly, which has a randomized layer structure on both sides and (ii) *Cyanophrys remus* butterfly, which has a polycrystalline structure on its ventral side.

The dorsal side of the *Albulina* butterfly is metallic blue, the ventral side is silvery green (cf. Fig. 8.7a). Figure 8.7a also shows the cross sectional TEM images, Fig. 8.7b is the binarized TEM image, and Fig. 8.7c is its Fourier power spectrum. The vertical structure $A^- - O - A^+$ corresponds to the layer structure. Note that there are two minima and one maximum between each pair of main peaks, which corresponds to the presence of three layers, as it was explained in Sect. 8.3, see Fig. 8.4. The peaks at A^- , A^+ are broadened horizontally because the layers are not perfectly flat but wavy. The vertical bars at B^- , B^+ correspond to the lateral order of the holes, cf. Fig. 8.5. These Fourier peaks have a finite thickness in both the horizontal and vertical direction because the holes are randomly arranged in the layers and the layers have different microstructure. The calculated spectrum is shown in Fig. 8.8c, together with the measured spectrum (Fig. 8.8b) and the schematics of the measurement setup (Fig. 8.8a). Measured and calculated spectra match extremely well.

The inset of Fig. 8.7c shows the Fourier image of an idealized structure, where the lateral order is perfect in the layers, but the layers are randomly displaced in the lateral direction. This corresponds to the model shown in Fig. 8.5. The spectrum of this ideal structure can be calculated easily by the Ewald construction and it is shown by the dotted line in Fig. 8.8c. This theoretical curve matches the trend of the peak positions calculated from the Fourier transform of the TEM section. Details of this calculation are given in Ref. [16].

Our example for the polycrystalline wing scale structure is the ventral side of the *Cyanophrys remus* butterfly. The ventral side of this butterfly (cf. Fig. 8.9a) has a dull, matt green color. Surprisingly, optical microscopy (cf. Fig. 8.9b) reveals (in reflection) that the overall matt, pea-green coloration of the ventral wings arises from the mixing of very tiny, bright, blue, green, and yellow spots

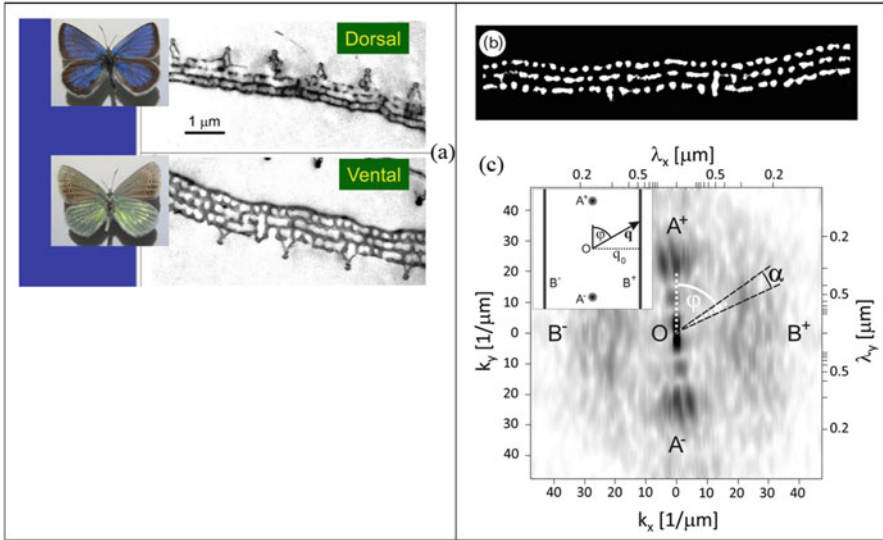


Fig. 8.7 Fourier analysis of the TEM images of the *Albulina metallica* butterfly. (a) Optical image of the dorsal and ventral side; cross sectional TEM images. (b) Processed TEM image of a ventral scale of *Albulina metallica*. A background correction and a binarizing filter was applied. (c) Fourier power spectrum of the processed TEM image. White corresponds to zero intensity and black to maximum intensity. Wave number (wavelength) scale is shown on the lower and left (upper and right) axis, respectively. The lines illustrate the procedure of the calculation of the backscattered spectrum from the Fourier image. The inset shows the Fourier image and the procedure of the spectrum calculation for a model image

randomly distributed over the scale. The dominant color and the intensity of the bright localized reflectors show a significant sensitivity to the observation and illumination directions, indicative of a local structural coloration. The SEM and TEM investigation of the wings [7] revealed scales with a rather peculiar structure: consisting of small grains with typical diameters in the 5–10 μm range. These grains show a regular structure, the regularity of the structure within one single grain is convincingly revealed by the cross-sectional TEM images in Fig. 8.9c. The grains act as individual photonic crystallites and, depending on the orientation of the incident light and the observation angle, give rise to the bright color spots detected in optical microscopy (cf. Fig. 8.9b). The summation of the colors and the random orientation of the grains may be responsible for the matt, pea-green coloration of the ventral scales.

As we explained in Sect. 8.3, the Fourier transform of a polycrystalline structure (cf. Fig. 8.6) is a ring like structure (a sphere in 3D), indicative of the presence of a radial order and no angular order. This Fourier image is similar to those obtained for photonic glasses and as was shown in the detailed analysis of Mainwald et al. [18], this structure leads to non-iridescent colors.

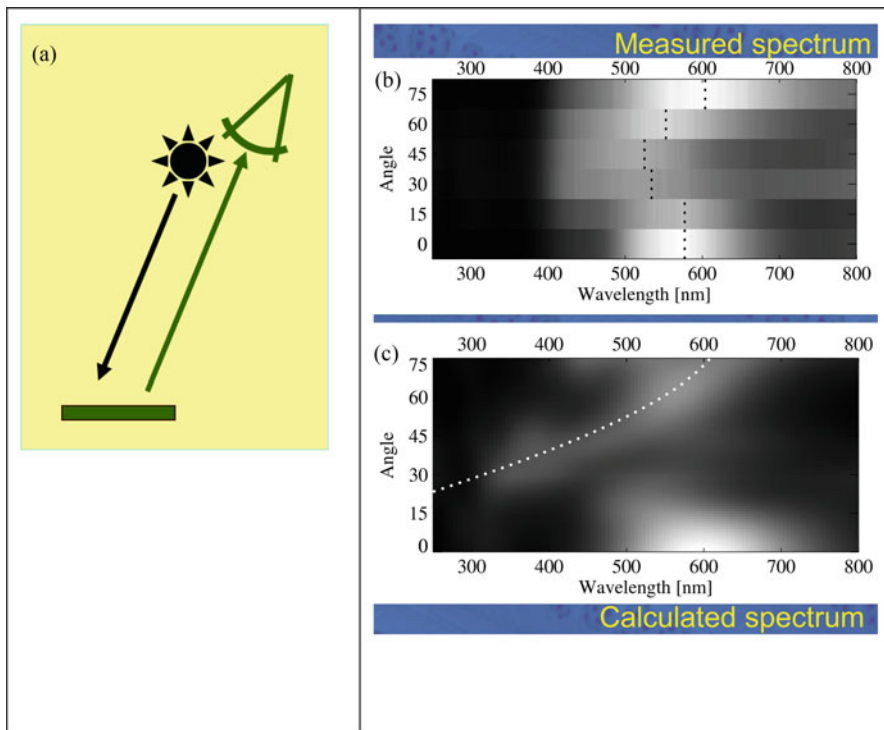


Fig. 8.8 Calculation of the backscattered spectrum and comparison to the measurement. (a) The backscattered measurement configuration. The illumination and the detector are placed at the same angle. (b) Reflectance spectrum of the *Albulina metallica* ventral (green) side recorded at backscattering arrangement at several angles. All spectra were measured relative to a diffuse white standard. Black corresponds to zero intensity and white to maximum intensity. A nonlinear gray scale is used to facilitate presentation. Black dotted lines show the wavelengths with maximum intensity for each angle. (c) Theoretical backscattered reflectance spectra calculated from the Fourier power spectrum shown on Fig. 8.7c. The dotted line shows the spectrum calculated for the model in Fig. 8.5

8.5 Signatures of Higher Order Scattering in the Optical Spectrum

In order to assess the validity of the first order approximation for the butterfly scales, we compared the first Born calculated spectra with an “exact” full 3D Finite Element (FEM) electro-dynamical calculation (<https://www.comsol.com/wave-optics-module>). The model structure consists of four layers. Each layer is an infinite square lattice of dielectric spheres. The lateral lattice constant is $d = 300$ nm and the layer distance is $a = 250$ nm. Figure 8.10a shows the unit cell used in the calculation. Free space boundary conditions were used at the $+z$ and $-z$ boundaries and Floquet periodic boundary conditions were applied in the lateral, $-x, +x, -y, +y$ directions.

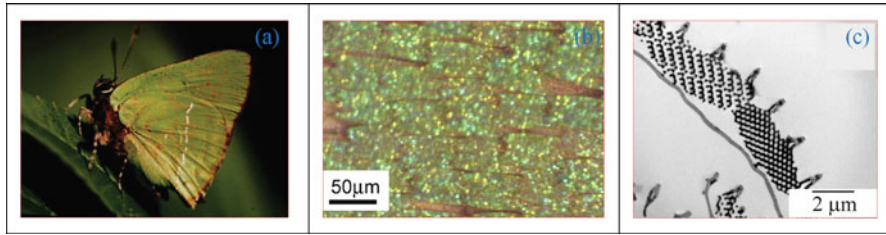


Fig. 8.9 Polycrystalline structure on the ventral size of the *Cyanophrys remus* butterfly. (a) The butterfly *Cyanophrys acaste* is shown here in a resting position, when the hind wing overlaps the forewing. The ventral faces of the wings are displayed, with a cryptic dull green color. *Cyanophrys remus* displays identical resting position. (b) Ventral surface of the wing. One may remark the occurrence of bright spots colored blue, green, and yellow, which light up with different intensities as the illumination and observation conditions change. (c) Crosssectional transmission electron micrograph through an individual green scale; one may notice the precise regular structure within one grain and the different orientation of the neighboring grains

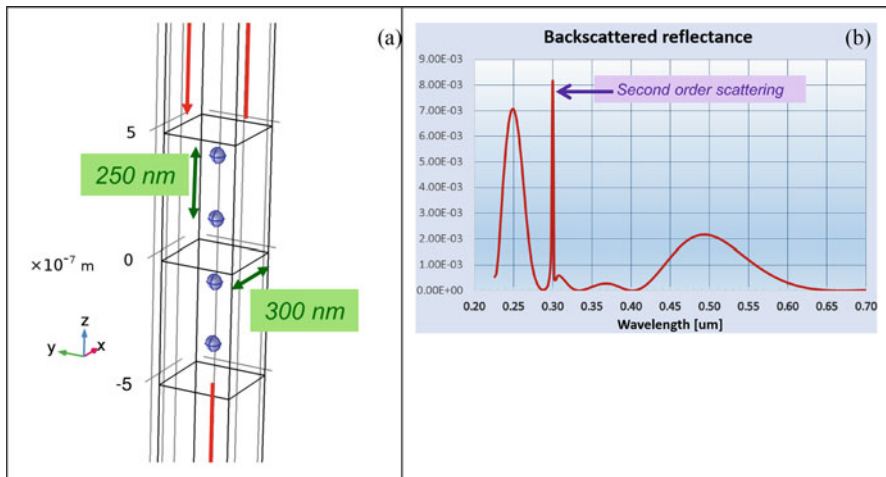


Fig. 8.10 Full 3D Maxwell equation calculation of the reflectance of a layered photonic nanostructure. (a) The unit cell of the calculation, containing four dielectric spheres of refractive index $n = 1.5$. The vertical distance of the spheres is 250 nm and the lateral size of the unit cell is 300 nm. The red arrows show the incoming, reflected, and transmitted wave vectors. (b) Calculated normal backscattered optical spectrum

Wave vectors of the incoming-, reflected-, and transmitted light are shown by red arrows. The incoming light arrives from the normal direction and the normal reflectance and transmittance was calculated as the function of the wavelength.

Figure 8.10b shows $R(\lambda)$, the normal reflectance as the function of wavelength. It has a wide peak around 500 nm, and another broadened, but sharper peak around 250 nm, two smaller intensity broad peaks between the two main peaks, and a sharp peak around 300 nm. The broad peaks can be reproduced by the first order scattering approximation, see Fig. 8.4 in Sect. 8.3. The main peaks of this spectrum

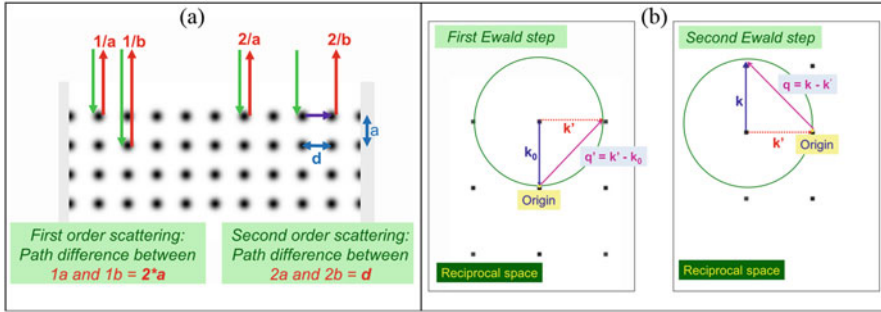


Fig. 8.11 First- and second order light scattering processes. (a) Real space lattice of four translation periodic layers with lateral periodicity d and layer distance a . The arrows show the light scattering processes, see the text for details. (b) Ewald sphere construction for the second order scattering in normal backscattered configuration. k_0 , k , and k' are the incoming, reflected, and intermediate wave vectors, respectively. See the text for details

are at $\lambda_j = 2dl/j$, where $j = 1$ is for the first harmonic peak and $j > 1$ for the higher harmonic peaks. Two main peaks fall into the UV-VIS wavelength window of our FEM calculation, the first harmonic peak at 500 nm and the second harmonic peak at 250 nm. The width of the two peaks is identical in k scale, but in λ scale the higher harmonic peaks are narrower, because of the reciprocal relation of k and λ . The two small peaks are the satellite peaks (cf. Fig. 8.4). The layer number is $n = 4$, hence we have $n-2 = 2$ satellite peaks.

Apart from the first order peaks explained above, the full 3D calculation (cf. Fig. 8.10b) reveals a very sharp peak at 300 nm. Note that this wavelength corresponds to the lateral lattice constant d . This peak is originated from the second order scattering, as explained in Fig. 8.11. Figure 8.11a compares the first- and second order light scattering processes. In the first order normal backscattering the electromagnetic field components scattered on each layer are coherently added. Two such components, denoted with 1a and 1b are shown on Fig. 8.11a, those scattered from the first- and the second layer. As we can see on the figure, the path difference of the two light components is $2a$, this defines the first order peaks. Light is scattered twice in second order processes. Such a process is shown by the vectors 2a and 2b. 2a is the component scattered by the first layer (same as 1a). Path 2b is a second order process. Light is first scattered on a sphere in the first layer and then on the adjacent sphere (at distance d) of the same layer, from where it is reflected back to the detector. The path difference of 2a and 2b is the lateral lattice constant, d , this gives rise to the peak at $\lambda = d = 300$ nm in Fig. 8.10b. This second order peak is sharp, because the structure is infinite in the lateral direction, contrary to the first order peaks, which are broad because of the finite vertical size of the system.

The two steps of the second order scattering are shown in Fig. 8.11b with the help of the Ewald construction. As was pointed out in [18], the probability of the second order scattering is the highest when the first order scattering direction is lateral, i.e. the scattered light remains inside the material for a long time, because it travels through the material parallel to the surface.

8.6 Conclusions

In this Chapter we invoked first order scattering theory in order to create a connection between the geometrical structure of butterfly wing scales and their optical spectrum. Optical spectrum of a butterfly scale is closely related to its reciprocal space structure. Indeed, butterfly scales are thin structures with moderate refractive index contrast, hence, the first Born approximation is applicable. Next we studied how order-disorder effects, which are always present in biological photonic nanostructures, influence their optical properties. A structure can deviate from a perfect long-range order in many different ways, i.e., there can be several kinds of randomnesses present in the structure. We analyzed in detail the effect of lateral- and vertical disorder, as well as polycrystalline disorder. The finite thickness of the butterfly scale causes a broadening of the spectral peaks and the appearance of small satellite peaks.

We also compared the first order scattering results with an exact electrodynamic calculation and identified the presence of second order processes, which cause the appearance of peaks in the UV part of the spectrum.

The simple reciprocal space approximation methods exposed in this chapter are useful because of their simplicity and tractable analytical properties. While exact calculations are readily available for periodic systems, the large unit cell necessary for modelling random structures has a high computational demand. First and second Born calculations can, however, easily handle large systems.

Acknowledgements This work was supported by the Hungarian NKFIH Grant Nos K 115724 and OTKA K 111741. G. I. M., and G. P. wish to thank the Hungarian Academy of Sciences and the Belgian FNRS for financial support.

References

1. Fox HM, Vevers G (1960) *The nature of animal colours*. Macmillan, New York
2. Berthier S (2007) *Iridescences: the physical colors of insects*. Springer, New York
3. Biró LP et al (2003) Role of photonic-crystal-type structures in the thermal regulation of a Lycaenid butterfly sister species pair. *Phys Rev E* 67:021907
4. Vukusic P, Sambles JR, Lawrence CR, Wootton RJ (1999) Quantified interference and diffraction in single Morpho butterfly scales. *Proc R Soc Lond B Biol Sci* 266:1403
5. Biró LP, Vigneron JP (2011) Photonic nanoarchitectures in butterflies and beetles: valuable sources for bioinspiration. *Laser Photonics Rev* 5:27
6. Kertész K, Molnár G, Vétesy Z, Koós AA, Horváth ZE, Márk GI, Tapasztó L, Bálint Z, Tamáska I, Deparis O et al (2008) Photonic band gap materials in butterfly scales: a possible source of “Blueparints”. *Mater Sci Eng B Solid-State Mater Adv Technol* 149:259. ISSN 0921-5107
7. Vukusic P, Sambles JR, Ghiradella H (2000) Optical classification of microstructure in butterfly wing-scales. *Photon Sci* 6:61
8. Ghiradella H (1998) *Microscopic anatomy of invertebrates*, vol 11A (Locke M (ed)). Wiley-Liss, New York, pp 257–287

9. Yablonovitch E (1993) Photonic band-gap structures. *J Opt Soc Am B Opt Phys* 10:283
10. Jin C, Meng X, Cheng B, Li Z, Zhang D (2001) Photonic gap in amorphous photonic materials. *Phys Rev B* 63:195107
11. Vukusic P, Sambles JR (2003) Photonic structures in biology. *Nature (London)* 424:852
12. Kertész K, Bálint Z, Vértésy Z, Márk GI, Lousse V, Vigneron J-P, Rassart M, Biró LP (2006) Gleaming and dull surface textures from photonic-crystal-type nanostructures in the butterfly *Cyanophrys remus*. *Phys Rev E* 74:021922
13. Bálint Z, Kertész A, Moser A, Kertész K, Biró LP, Parker AR (2008) A supposition: structural colours resulting from both natural and sexual selection on an individual wing in the butterfly genus *Cyanophrys* (Lepidoptera: Lycaenidae). *Ann Hist-Natur Mus Nat Hung* 101:63
14. Taflove A, Hagness S (2005) Computational electrodynamics: the finite-difference time-domain method. Artech House Publishers, Norwood
15. Benedek GB (1971) Theory of transparency of the eye. *Appl Opt* 10:459
16. Márk G, Vértésy Z, Kertész K, Bálint Z, Biró L (2009) Order-disorder effects in structure and color relation of photonic-crystal-type nanostructures in butterfly wing scales. *Phys Rev E Stat Nonlinear Soft Matter Phys Rev E* 80(5 Pt 1):051903
17. Prum RO, Quinn T, Torres RH (2006) Anatomically diverse butterfly scales all produce structural colours by coherent scattering. *J Exp Biol* 209:748
18. Maiwald L, Lang S, Jalas D, Renner H, Petrov AY, Eich M (2018) Ewald sphere construction for structural colors. *Opt Express* 26:11352–11365